Dyes and Pigments 173 (2020) 107932

Contents lists available at ScienceDirect

Dyes and Pigments

journal homepage: http://www.elsevier.com/locate/dyepig

BODIPY-based organic color conversion layers for WLEDs

Hurriyet Yuce [a], Tugrul Guner [a], Suay Dartar [b], Beraat U. Kaya [b], Mustafa Emrullahoglu [b,**], Mustafa M. Demir [a,*]

[a] Department of Materials Science and Engineering, Izmir Institute of Technology, Turkey
[b] Department of Chemistry, Izmir Institute of Technology, Turkey

ARTICLE INFO

Keywords:
Electrospinning
Fiber composite
PDMS
BODIPY
White light
Phosphor-converted wled

ABSTRACT

The usage of organic dyes in phosphor conversion layer of WLED is an attractive approach since they have high molar extinction coefficient and photostability. Various types of organic pigments have been employed for this purpose such as BODIPY, perylene diimide, Rhodamine B, pyrene, Nile red, etc. Among those, BODIPY-based organic dyes appear to be promising candidate for white light generation. In this work, for the first time, red and green emitting BODIPY-based organic molecules have been used as colour conversion layer. These molecules were associated with PMMA in DMF solution and the resulting solution was subjected to electrospinning. Colorful electrospun mats were embedded into PDMS matrix and their free-standing PDMS composite films were used as color conversion layers over blue LED to produce white light such that CRI of 95 and CCT of 4200 K was achieved. These values show that BODIPY-based organic molecules containing fiber composites are promising candidates to be used as color conversion layers for white light applications.

1. Introduction

Producing white light with light-emitting diodes (LEDs) is considered to be a promising strategy for future lighting [1–4]. Compared to traditional lighting products (i.e. incandescent and fluorescent bulbs), LED-based lighting can provide significantly more energy-efficient and long-lasting products [5–7]. One can produce LED based white light either through multi-chip configuration or phosphor-conversion [1,3,8–10]. The former includes a configuration consisting of red-green-blue (RGB) LED chips individually to satisfy main colours [11]. However, such a design suffers from complexity due to changing individual response of LED chips against temperature and aging, which causes instability for the generated white light in terms of its optical features. The latter contains a colour conversion layer consisting of mainly phosphors [8,12–16] which are placed over a blue or UV LED chip. This strategy, which is known as phosphor-converted white LED (pc-WLED), is a typical design that has been already used in commercial products today [17,18].

Depending on the material used in colour conversion layer, optical features of the produced white light can vary. For instance, mainstream design of pc-WLED consists of well-known yellow phosphor *cerium doped yttrium aluminium garnet* (YAG:Ce^{3+}) and a blue LED chip. This system can produce white light with adequate *Color Rendering Index* (CRI) (<80) and high *Correlated Color Temperature* (CCT) (>6000 K). In order to increase CRI and decrease CCT, one can integrate red phosphors into the system [16,19,20]. On the other hand, apart from the phosphor usage, various luminescent materials such as quantum dots [21], perovskites [22–28], and organic dyes [29–35] can be employed as color conversion layers. Among those, organic dyes have been studied already in organic LED (OLED) devices [36–39] and as colour conversion layer over LED to generate white light to satisfy desired optical features. Much effort has been made from the researchers in order to incorporate organic dyes into several polymeric matrices like poly(methyl methacrylate) (PMMA) [30,40], and polystyrene (PS) [29,31].

Using organic dyes as color conversion layers over blue or UV LED to produce white light is a promising strategy [29,35,41], but they suffer from aggregation-caused quenching due to strong π-π interactions [42–45], relatively poor photochemical and thermal stabilities mainly [46,47]. In order to avoid from these issues, several methods have been proposed already. Electrospinning appears to be a facile technique [48] that can prevent the aggregation of organic dye molecules even they are distributed in polymer solvents. For instance, our group has demonstrated lately that the producing PS fibers in the presence of perylene diimide and its derivatives can prevent the formation of further

* Corresponding author. Department of Materials Science and Engineering, Izmir Institute of Technology, Izmir, Turkey.
** Corresponding author. Chemistry Department, Izmir Institute of Technology, Izmir, Turkey.
E-mail addresses: mustafaemrullahoglu@iyte.edu.tr (M. Emrullahoglu), mdemir@iyte.edu.tr (M.M. Demir).

https://doi.org/10.1016/j.dyepig.2019.107932
Received 5 February 2019; Received in revised form 19 March 2019; Accepted 26 September 2019
Available online 27 September 2019

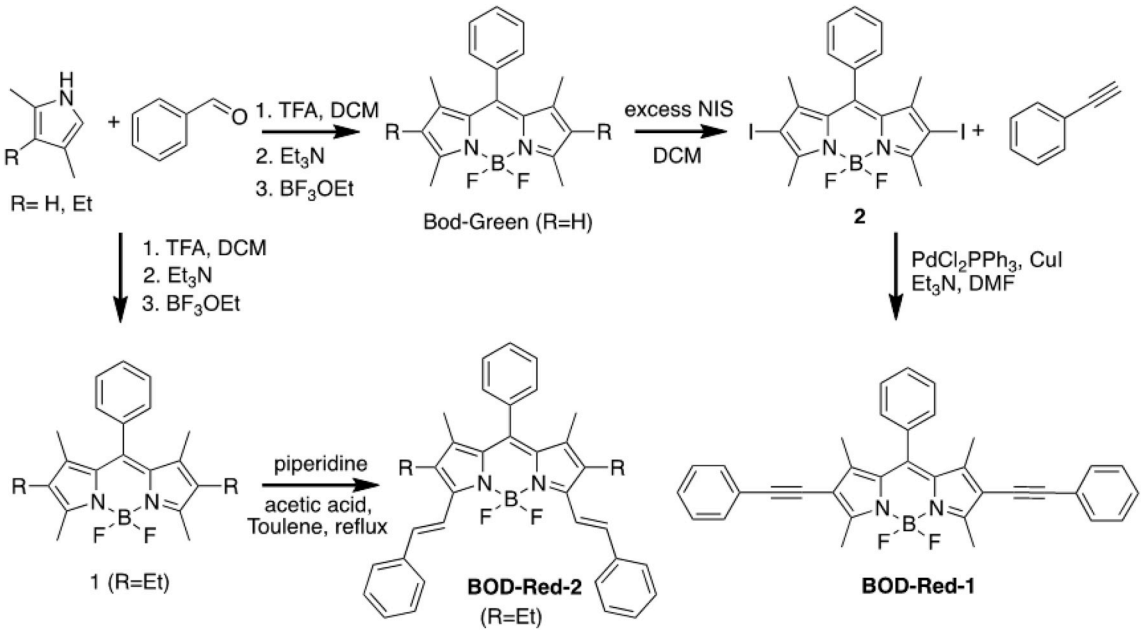

Fig. 1. Synthesis of BOD-Green, BOD-Red-1 and BOD-Red-2.

aggregation compared to the corresponding perylene diimide solutions [29]. Another possible method involves the development of organic dyes providing aggregation-induced emission [43,49], which shows intense emission in the solid state, or fluorophore functionalized mesoporous silica can designed for the stability improvement of these organic dyes [50,51].

The search for new classes of fluorophores showing reduced aggregation-caused quenching for potential applications in LED research has intensified significantly in the past few years. As a bright fluorescent dye with sharp absorption/emission bands, high molar extinction coefficients (even larger than 80.000 M^{-1} cm^{-1}), high fluorescence quantum yield greater than 0.50, the BODIPY fluorophore, has gained great importance recently in diverse applications such as chemosensors [52–54], dye lasers [55,56], photosensitizers [57,58], photodetection [59], sensitizers for solar cells [60], energy-transfer cassettes [61–63], light harvesters [64,65] and fluorescent organic devices [66,67]. To the best of our knowledge, the utilization of BODIPY-dyes for a purpose specifically of white light emission applications have not yet to be explored. To this end, we designed and synthesized three BODIPY derivatives with different photo-physical properties and investigated their potential for use in white light emitting systems.

In this study, green- and red-emitting BODIPY-based organic dyes were fabricated, and then PMMA/BODIPY-based organic dyes were produced in the form of fibers in order to use them as color conversion layers over blue LED. Initially, green-emitting BODIPY (BOD-Green) was employed over LED, and resulting white light properties were examined. Then, two red-emitting BODIPY (BOD-Red-1, and BOD-Red-2) were integrated into the same system containing fixed amount of BOD-Green fiber to improve CRI, LER and reduce CCT. Finally, varying amounts of both BOD-Green, BOD-Red-1, and BOD-Red-2 fibers were produced as color conversion layers and their white light properties were compared with the same amount of commercial red phosphor containing polydimethylsiloxane (PDMS)/BOD-Green fiber composites.

2. Experimental

2.1. Materials and methods

BODIPY having basic colours (BOD-Green, BOD-Red-1 and BOD-Red-2) were synthesized in order to be employed as color conversion layers for the white light generation. The synthesis scheme of BODIPY-based dyes is given in Fig. 1, and the synthesis procedure of the dyes together with their corresponding nuclear magnetic resonance (NMR), mass spectra analysis, and quantum yields can be found in detail in the supporting information. PL and absorption measurements were performed via an integrating sphere (ISP-50-80-R, Ocean Optics Inc.) connected to a USB2000 + spectrometer (Ocean Optics Inc., Dunedin, FL, USA) with a premium fiber cable. As a blue light source, a commercial blue LED chip (CREE, 450 nm, Royal Blue) was used. Morphology of BOD-Green fibers was analysed by scanning electron microscopy (SEM; Quanta 250, FEI, Hillsboro, OR, USA). Confocal microscopy system (1X71 Olympus Microscope equipped with Andor Revolution System) was used to obtain appearance of BOD-Green fibers under 488 nm laser light. In addition, CRI, CCT, Lumen, and LER were calculated, and CIE color coordinate diagram was determined by using ColorCalculator Programme, OSRAM.

2.2. Fabrication of BODIPY-based organic dye containing PMMA fibers (PMMA-BODIPY)

BODIPY solution was prepared as 3 g in 10 mL dimethylformamide (DMF). PMMA solution was prepared with the mixture of 2 g PMMA and 10 mL DMF. Then, 2 mL of PMMA solution with 0.5 mL BODIPY solution was mixed in a glass vials. These two mixture solutions were subjected to electrospinning. During the fabrication of fibers, the parameters of electrospinning were fixed at 20 kV and 1 mL per hour of flow rate. Since there is a potential difference between the syringe tip and the aluminium foil, which is used as a collector, BODIPY and PMMA solution jet was ejected. Solvent evaporation leaves behind PMMA-BODIPY fibers. The fibers were then removed from the aluminium foil used as free standing film.

2.3. Fabrication of fibrous PDMS/PMMA-BODIPY composites

Fabricated BODIPY fibers were placed into a metal mold with the thickness of 0.2 cm and the radius of 2.0 cm. Then, prepared PDMS with 10:1 ratio of oligomer to curing agent was dropped over the fibers placed into the metal mold. The weight of the fibers was changed ranging from 10 mg to 50 mg with the constant weight of PDMS (1 g). The mold was

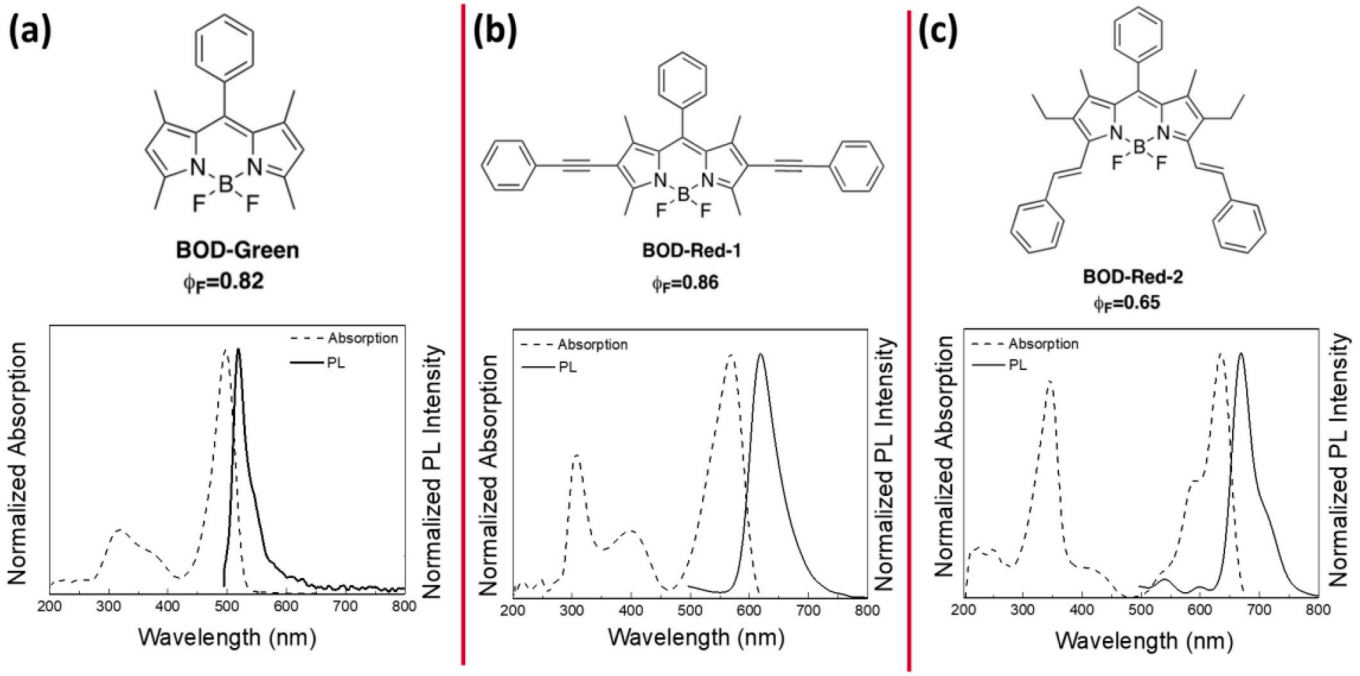

Fig. 2. Structure of green and red emitting BODIPY-based fluorophores and their PL and absorption measurements. (For interpretation of the references to color in this figure legend, the reader is referred to the Web version of this article.)

kept under vacuum during 30 min to extract evaporated solvent from the sample. Then, the mold was cured at 70 °C during 20 min to be cross-linked of the polymers. Then, it was removed from the mold after the sample cool down at room temperature.

3. Results and discussion

3.1. Colorful BODIPY molecules (BOD-Green, BOD-Red-1, and BOD-Red-2)

Absorption and photoluminescence (PL) spectra of the BOD-Green in DMF solution were measured, and the results are presented together with its molecular structure, and fluorescence quantum yield (Φ_F) in Fig. 2a. BOD-Green was found to have two distinct and clear absorption signals (black dashed line); one at 497 nm, and another at 318 nm. The one at the higher wavelength has a narrower width having almost 40 nm. On the other hand, the one at the lower wavelength indicates that it has a broader width at around 100 nm, and having intensity equal to quarter of the previous absorption peak at the higher wavelength. Moreover, the second signal at the lower wavelength may be the result of the merging two different absorption signals; at 318 nm and at 369 nm. This merging two absorption signals may be the result of such a high widening observed for the lower wavelength signal. For PL spectrum, presented with black solid line, BOD-Green was excited with a blue LED chip having 450 nm. It was observed that emission of the BOD-Green has a single peak having narrow full width half maximum (FWHM) of ~39 nm, and it reaches its highest intensity around 520 nm.

Red dyes (BOD-Red-1 and BOD-Red-2) have different characteristic molecular structures, and absorption and emission signals (collected at 450 nm excitation wavelength) (Fig. 2b-c). For the former case, molecular structure of the BOD-Red-1, and its corresponding fluorescence quantum yield (Φ_F) are presented together with its absorption and emission signals in Fig. 2b. This structure shows three main distinct absorption signals at 307 nm, 400 nm, and 570 nm. On the other hand,

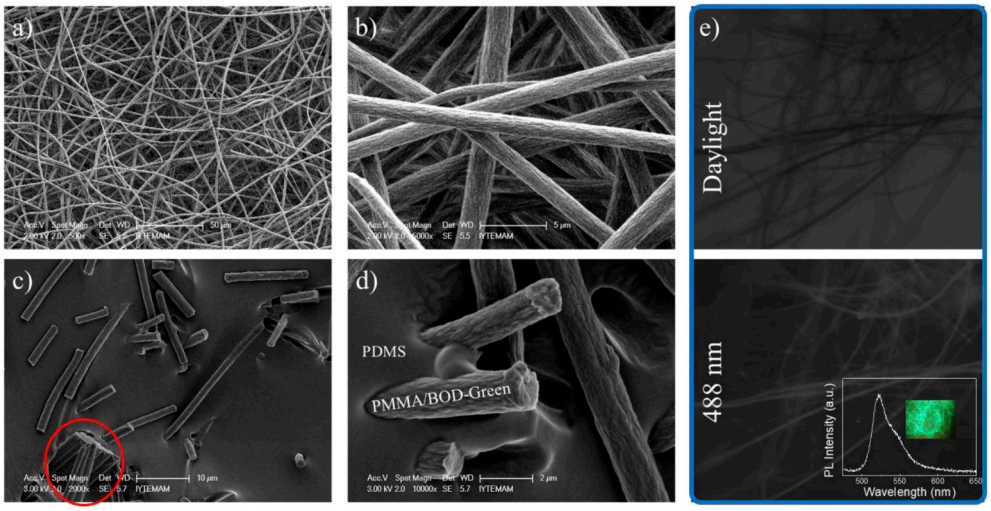

Fig. 3. SEM images of the produced PDMS/PMMA-(BOD-Green) green fibers at **a)** 500x, and **b)** 5000x magnifications. **c)** and **d)** present the cross-section of PDMS/PMMA-(BOD-Green) composite films. **e)** presents the confocal microscope images of the fibers under daylight (top) and 488 nm laser illumination (bottom). Inset shows the PL spectrum of the prepared fibers under 450 nm blue LED excitation and appearance of the emitting fibers (photographically) in confocal microscope. (For interpretation of the references to color in this figure legend, the reader is referred to the Web version of this article.)

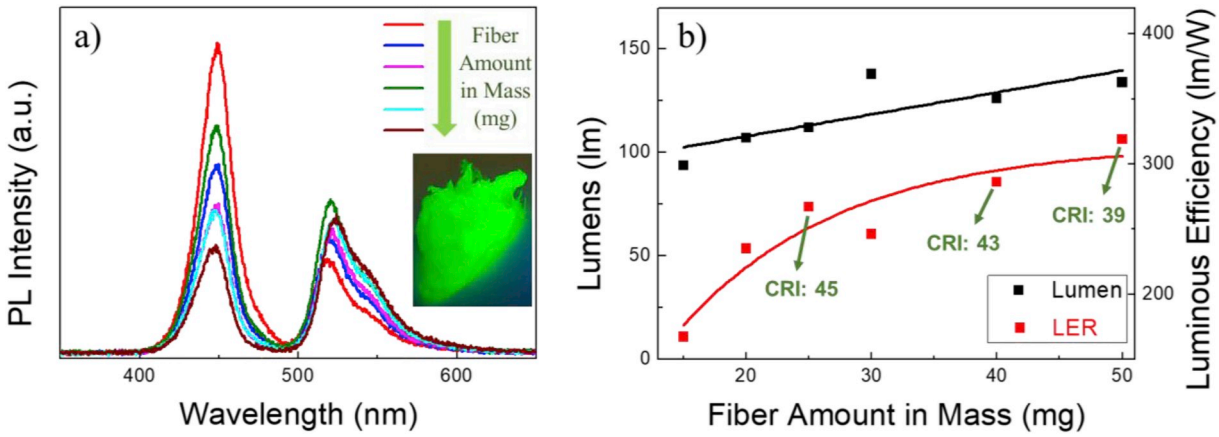

Fig. 4. a) Spectrum, and **b)** white light properties, in terms of lumens, luminous efficiency and CRI, of the produced PDMS/PMMA-(BOD-Green) composites as color conversion layers over blue LED chip. Inset given in **a)** demonstrates the appearance of PMMA-(BOD-Green) fibers under UV illumination.

there is a narrow single emission at 620 nm with FWHM of 55 nm under 450 nm excitation. For the second case, BOD-Red-2, its molecular structure and fluorescence quantum yield (Φ_F) (Fig. 2c) indicate that there is a significant difference between BOD-Red-1 and BOD-Red-2. This structural difference causes a change in the absorption and emission signals of the resulting dye compared to BOD-Red-1. Dashed line shown in Fig. 2c presents that there are two different main absorption signals at 345 nm and 635 nm. Second absorption signal at 635 nm have also a shoulder at 590 nm, which may indicate the existence of an additional molecular state apart from the main peaks described above. Meanwhile, there is almost a single emission signal at 670 nm with FWHM ~42 nm presented with solid line, which is obtained under 450 nm excitation. There is a shoulder-like broadening of this emission signal at 707 nm, this result may hint about the presence of another radiative energy transfer path in addition to one correspond to main emission peak at 670 nm. Compared to BOD-Red-1, this molecule has red-shifted emission peak, which is 8%, indicating a reduction in the gap between energy levels responsible from the radiative energy transfer.

3.2. PMMA-BODIPY fibers and PDMS/PMMA-BODIPY composites

To explore the morphology of the fabricated PMMA-BODIPY fibers, PMMA-(BOD-Green) was selected as representative sample, and corresponding SEM images are demonstrated in Fig. 3a-b. At lower magnification in Fig. 3a, SEM image presents that there is an explicit formation of fibers distributing homogenously throughout the image. At higher magnifications (Fig. 3b), the surface of these fibers was observed, as they are almost smooth along its length. Moreover, the resulting fibers are observed to have diameters ranging from 1.4 to 2.0 μm. SEM images taken from the cross-section of the produced PDMS/PMMA-(BOD-Green) fibers composite film at several magnifications are presented in Fig. 3c-d. Both images show that the fibers preserve their morphology even they are coated with PDMS. At higher magnification (Fig. 3c), some of the fibers seem damaged during the sample preparation; however, region that was taken into circle suggest that the fibers are aggregated and packed into an ordered structure along the PDMS matrix. On the other hand, individual fibers are also captured as demonstrated in Fig. 3d, and the morphology is preserved in the PDMS matrix as already demonstrated. The distribution of BOD-Green throughout the fiber volume was investigated via confocal microscopy. Corresponding images of the fibers under both daylight and 488 nm laser illumination are shown in Fig. 3e. Before illumination, optical images of the fibers were collected at 10x magnification. These images confirm the ones that taken by SEM in the sense of smooth fiber formation, which are appearing as dark regions over the grey background, having comparable diameters close to each other. After exciting these fibers with 488 nm lasers, the dark regions belonging to fibers begin to shine. The bright regions appear that the result may indicate the presence of (BOD-Green)-rich regions (Fig. 3e). Since the focus region of the microscope is restricted with particular depths and field of view, it is expected to observe different brightness level for these fibers. On the other hand, by tracking a single fiber in the image, one can observe that there is a homogenous distribution of brightness, which may hint about the homogenous dispersion of BOD-Green. Inset of Fig. 3e presents the typical emission of these fibers under 450 nm blue LED illumination. The peak position and FWHM of the resulting emission are almost identical with the one of the solution (Fig. 2). A significant aggregation of BOD-Green molecules in the presence of PMMA was not observed throughout the entire sample. Photographic image of the emitting fibers captured from the optical microscope is presented in the inset of PL spectra. The fibers show an explicit homogenous green emission from the fibers and their intensity gets higher at the stacking fiber regions.

3.3. White light properties of the PDMS composite films prepared by merely BOD-Green

Similar to the mainstream design of YAG-based phosphor-converted white LED configuration, green-emitting BOD-Green fibers were employed over 450 nm blue LED chip as color conversion layer to produce white light since BOD-Green has an absorption range covering the emission of LED chip. Photographic image of the PMMA-(BOD-Green) fibers under 254 nm UV illumination presented at the inset. This free-standing mat of the fibers shows a clear and intensive green emission distributed homogenously. In order to obtain them in the form of colour conversion layer, the fixed amount of PDMS was casted over PMMA-(BOD-Green) fibers in varying fiber masses.

PL spectrum was registered individually over blue LED chip, and presented in Fig. 4a. Two emission signals belonging to blue LED (at 450 nm) and BODIPY (at 520 nm) were maintained in the presence of PDMS medium since PDMS keeps its transparency even after cross-linking. As the amount of fiber increases, the highest intensity of the peak corresponding to blue emission from LED chip at 450 nm remarkably decreases. Meanwhile, the emission of the PMMA-(BOD-Green) fibers rises due to interaction of more BOD-Green molecules with the incoming blue light. Reducing the blue emission while increasing the PMMA-(BOD-Green) emission is the natural outcome of increasing fiber amount since more fibers in mass means more BOD-Green molecules can interact with the blue light.

White light quality of the resulting (BOD-Green)-based colour conversion layers was investigated through exploring their lumens, LER, and CRI depending on the varying fiber mass (Fig. 4b). For the lumens, it increases surprisingly (this parameter fits well to linear curve) from 94

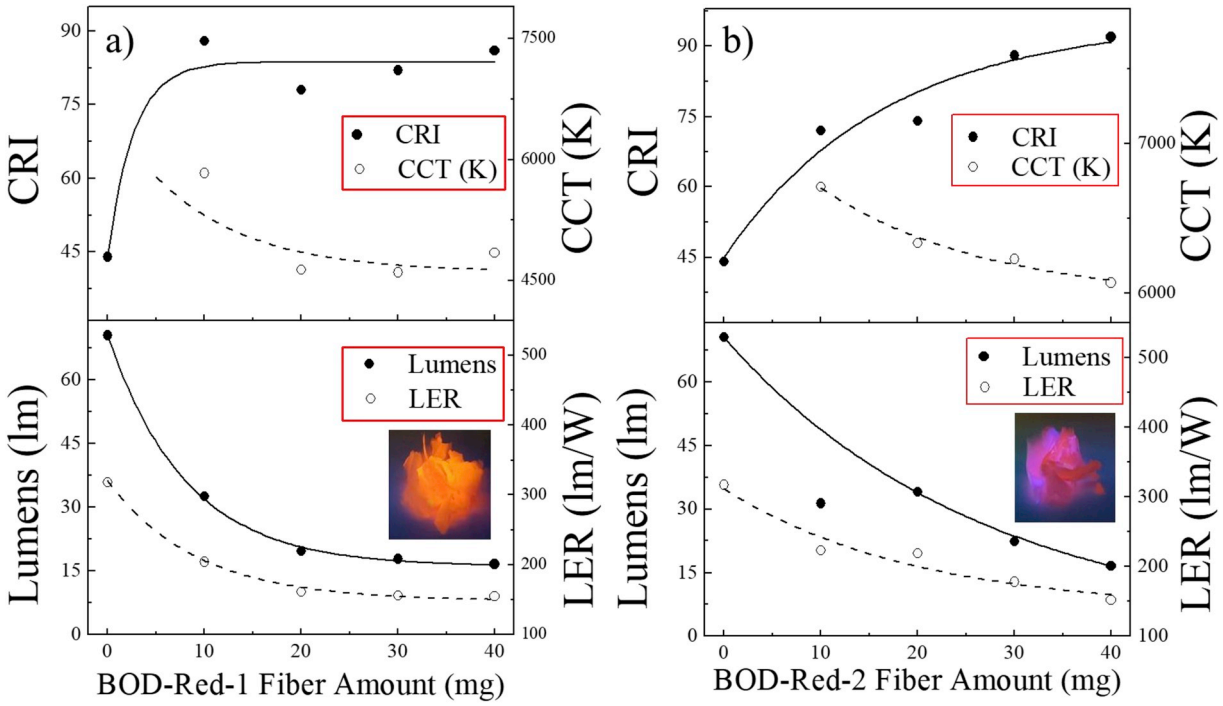

Fig. 5. CRI, CCT, lumens, and LER of the generated white light in the presence of varying amount of red-emitting **a)** BOD-Red-1, and **b)** BOD-Red-2 fibers in terms mass (mg) together with fixed amount of BOD-Green fibers (20 mg). (For interpretation of the references to color in this figure legend, the reader is referred to the Web version of this article.)

lm to 134 lm (43% enhancement) as the fiber amount in mass increases from 15 mg to 50 mg. Introducing more fibers into the system is expected to increase the optical path length (total path that photon takes during its motion throughout the system), which should lead to a decrease in lumens. Such a rising in lumens depending on the fiber amount may be due to improved intensity of the BOD-Green emission based on the enhanced multiple-scattering of light together with the increased amount of BOD-Green molecules contributing to emission. Such a scattering-based enhancement in the emission intensity was already verified for phosphors in our previous studies [68,69]. LER follows an exponential decaying pattern, and even though it saturates after 50 mg, it enhances dramatically in total as the fiber mass increases, from 157 lm/W to 319 lm/W showing almost ~90% improvement. Such a high improvement is the result of increasing green emission from the PMMA-(BOD-Green) fibers. However, CRI of these samples (green arrows) was obtained far below the satisfactory levels, and systematically decreases as the fiber amount increase.

3.4. White light properties of the PDMS composite films prepared by BOD-Green and red-emitting BOD-Red-1 or BOD-Red-2 dyes

To overcome the issue of having low CRI, two different red-emitting BODIPY-based dyes were integrated into PMMA fibers. These red-emitting PMMA-(BOD-Red-1) and PMMA-(BOD-Red-2) fibers were then stacked over the fixed amount of green-emitting PMMA-(BOD-Green) fibers (20 mg) in varying amounts in terms of mass from 10 mg to 40 mg. Colour conversion layer was obtained by pressing these stacked fibers between two glass slides in this case rather than casting PDMS over them. White light properties of the colour conversion layers composing of green-emitting PMMA-(BOD-Green) and red-emitting PMMA-(BOD-Red-1) and PMMA-(BOD-Red-2) fibers are presented in Fig. 5. The order of the stacked fibers is crucial in order to obtain high emission intensity for the red-emitting ones since their quantum efficiencies, in the form of fiber, are below the adequate level to get significant red emission. Therefore, PMMA-(BOD-Red-1) or PMMA-(BOD-Red-2) fibers were put over the PMMA-(BOD-Green) fibers in order to be excited additionally by the green emission (520 nm) of BOD-Green. Therefore, this configuration enables the excitation of either BOD-Red-1 or BOD-Red-2 through two different wavelengths; one from the BOD-Green emission at 520 nm and the other one from the blue LED chip at 455 nm at the same time. Fig. 5a shows the variation of CRI, CCT, lumens, and LER of the resulting white light depending on the varying BOD-Red-1 fiber amount over the PMMA-(BOD-Green) fibers. Inset photograph demonstrates the orange emission of PMMA-(BOD-Red-1) fibers under 254 nm UV illumination. Compared to neat PMMA-(BOD-Green) fibers, CRI improves dramatically as the BOD-Red-1 fibers introduced into the system initially (10 mg), from 45 to 88, providing % 96 enhancement. As the amount of BOD-Red-1 fiber increases, CRI follows almost a stable line around 83. Meanwhile, CCT drops from very high temperatures (>50,000 K) at 0 mg to a satisfactory level, which is 5800 K at 10 mg and follows a decaying pattern where it saturates around 4600 K according to the fitted curve. Note that this combination is close to the one of daylight. Meanwhile, both lumens and LER of the resulting white light obtained from BOD-Red-1 employed colour conversion layers follow a decaying pattern as the BOD-Red-1 fiber amount increases, which is expected for lumens since the addition of fibers either scatters the incoming blue light more or leads to a significant increase for the optical length throughout the sample. Compared to previous case (Fig. 4b), where the enhanced multiple scattering of light lead to increase in the lumens, BOD-Red-1 dyes employed over PMMA-(BOD-Green) fibers absorb both blue light from the LED chip and from the emission of BOD-Green fibers, and in return, emit with lower intensities due to their low quantum efficiencies in the form of fibers. Therefore, it makes sense that lumen decays as the BOD-Red-1 fiber amount in mass increases (from 320 lm/W (neat PMMA-(BOD-Green) at 0 mg) to 150 lm/W at BOD-Red-1 fiber amount having 40 mg). On the other hand, the reason for the decay of LER can be explained via the decreasing green-emission since adding more PMMA-(BOD-Red-1) fibers absorb more green emission from PMMA-(BOD-Green) fibers (PL spectrum of the samples composing of BOD-Green and BOD-Red-1 fibers are presented in Fig. S1). Reduced green region causes a significant decrease for LER since the luminosity function follows a Gaussian-like pattern where it

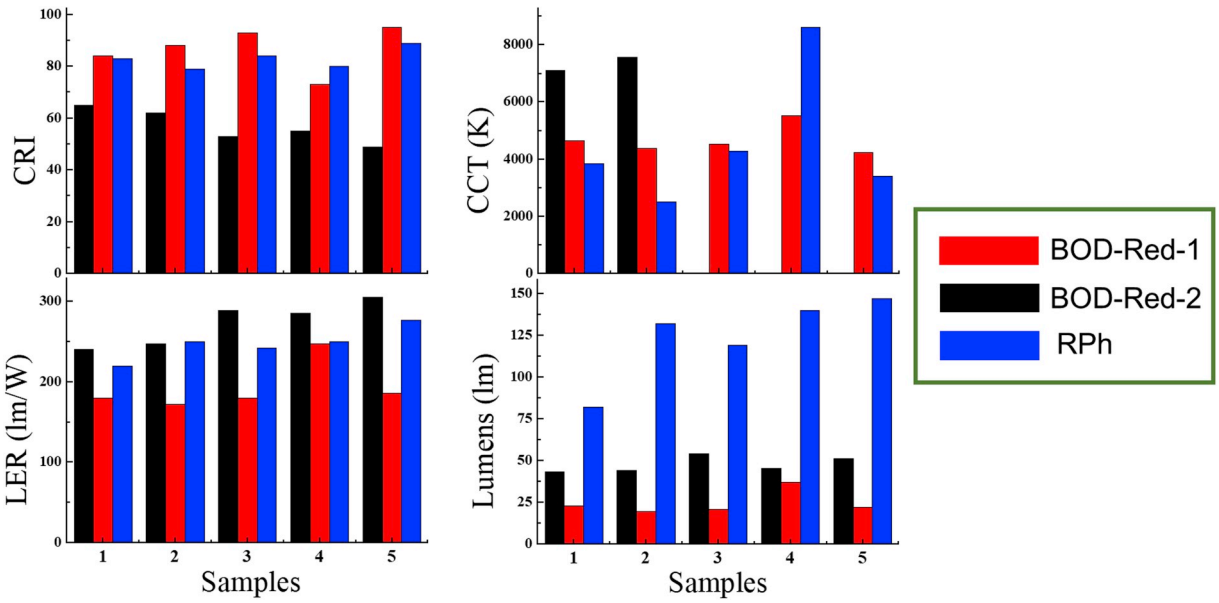

Fig. 6. Comparison of CRI, CCT, LER, and Lumens that are obtained from the generated white light through different five sample series. These samples consist of varying amount of BOD-based fibers and inorganic red phosphors (Table S1). Here, for each sample series, the amounts of BOD-Red-1, BOD-Red-2 fibers and RPh (red phosphor) are kept as the same. (For interpretation of the references to color in this figure legend, the reader is referred to the Web version of this article.)

gets its highest value for the green region. For the case of PMMA-(BOD-Red-2) fibers, the same sample preparation procedure described above has been followed. Fig. 5b shows the resulting optical features including CRI, CCT, lumens, and LER of the produced white light by employing PMMA-(BOD-Red-2) fibers over fixed amount of PMMA-(BOD-Green) fibers (PL spectrum of these samples are given in Fig. S2). The inset of the figure demonstrates the photographic image of the PMMA-(BOD-Red-2) fibers under 254 nm UV illumination, which appears as a dark red colour. When the PMMA-(BOD-Red-2) fibers introduced into system (10 mg), CRI improves significantly from 45 to 72 (60%). Even though this increase is dramatic, it is lower than the sample containing PMMA-(BOD-Red-1) fibers at 10 mg. However, CRI shows an explicit increase, which can be followed by a pattern fitted well to exponential decay. Unlike the saturating-like behaviour of PMMA-(BOD-Red-1) fibers around the CRI of 83 (Fig. 5a), the ones containing BOD-Red-2 shows a decaying increase, and even reach to 92 (%104) at 40 mg. Meanwhile, similar to previous case (PMMA-(BOD-Red-1) fibers), CCT becomes valid after introducing the BOD-Red-2 fibers into the system, and it decays from 6700 K to 6100 K as the amount of BOD-Red-2 fibers increases. Compared to PMMA-(BOD-Red-1) fibers, CCT obtained by using PMMA-(BOD-Red-2) fibers produced cooler white light, almost 2000 K more than the ones containing BOD-Red-1. Both lumens and LER follow an exponential decay due to the aforementioned reasons while describing the white light properties of the samples composing of PMMA-(BOD-Red-1) fibers. However, the decay pattern of this system shows the lumens and LER will continue to decay even after the BOD-Red-2 fiber amount of 40 mg unlike the previous case, where BOD-Red-1 containing fibers saturate after 20 mg. This may indicate that integration of the PMMA-(BOD-Red-2) fibers into the system can require more fibers in order to reach saturation in terms of all optical features including CRI, CCT, lumens, and LER since all are maintaining either their decrease or increase even after the 40 mg.

In order to determine the use of either BOD-Red-1 or BOD-Red-2 as colour conversion layer together with green-emitting PMMA-(BOD-Green) fibers over blue LED chip is whether commercially viable or not, these samples were subjected to also varying amount of PMMA-(BOD-Green) fibers. Moreover, commercial inorganic red phosphor was also integrated into PMMA-(BOD-Green) fiber system through casting PDMS/inorganic phosphor over these fibers, and the sample labelled as RPh. The details of the mass of the employed fibers, which are labelled as Sample x (x ranges from 1 to 5), are given in Table S1. PL spectra of the corresponding samples are presented in Fig. S3. The intensity of the green emission from PMMA-(BOD-Green) fibers gets the lowest at the highest amount of BOD-Red-1 and BOD-Red-2 fiber employed in a system composing of stacked PMMA-(BOD-Green) and PMMA-(BOD-Red-1) or PMMA-(BOD-Red-2) fibers. Optical features of the generated white light of the samples composing of either BOD-Red-1, BOD-Red-2 or RPh are presented in Fig. 6. The optical results in terms of CRI, CCT, LER, and Lumens presented in Fig. 6 were calculated by using ColorCalculator Programme, OSRAM by applying it to the collected PL measurements. Driving current of blue LED was kept constant as 150 mA while recording the corresponding PL spectrum of these samples. Having the same amount of BOD-Red-1 shows better CRI almost every sample compared to RPh, and it even reaches to 95 (Sample 5) with CCT of 4200 K while RPh can reach to 89 with CCT of 3400 K maximally at the same fiber amounts. Meanwhile, BOD-Red-2 containing samples provide inadequate CRI levels around 50 almost at all varying fiber amounts. In terms of CCT, RPh shows that the samples prepared by inorganic phosphor provide a warm white light since it can show significantly lower color temperatures. For instance, sample 2 of RPh gets 2500 K while the sample of BOD-Red-1 provides 4400 K, and BOD-Red-2 does 7500 K. However, CCT of the samples containing PMMA-(BOD-Red-2) fibers have no valid CCT values at higher PMMA-(BOD-Green) fiber amounts (sample 3, 4, and 5). Meanwhile, PMMA-(BOD-Red-1) fibers provide CCT of ~4700 K in average, which is close to the average obtained from RPh of ~4500 K. In the case of LER, even though the BOD-Red-2 containing samples provide the lowest CRI and inadequate CCT, they are able to provide the highest LER including all samples while the ones containing BOD-Red-1 shows the lowest. The fibers composing of PMMA-(BOD-Green) and PMMA-(BOD-Red-2) reach 305 lm/W for sample 5 while the ones containing BOD-Red-1 shows 186 lm/W, and RPh 277 lm/W. However, in terms of lumens, the samples containing inorganic red phosphors show dramatically higher values compared both BOD-Red-1 and BOD-Red-2 containing samples, where BOD-Red-1 is still providing the lowest levels for lumens. This may be the result of very high emission intensity obtained from the inorganic red phosphors (Fig. S3) due to its high quantum efficiency (~90%).

Meanwhile, a color conversion layer composing of BOD-Green and

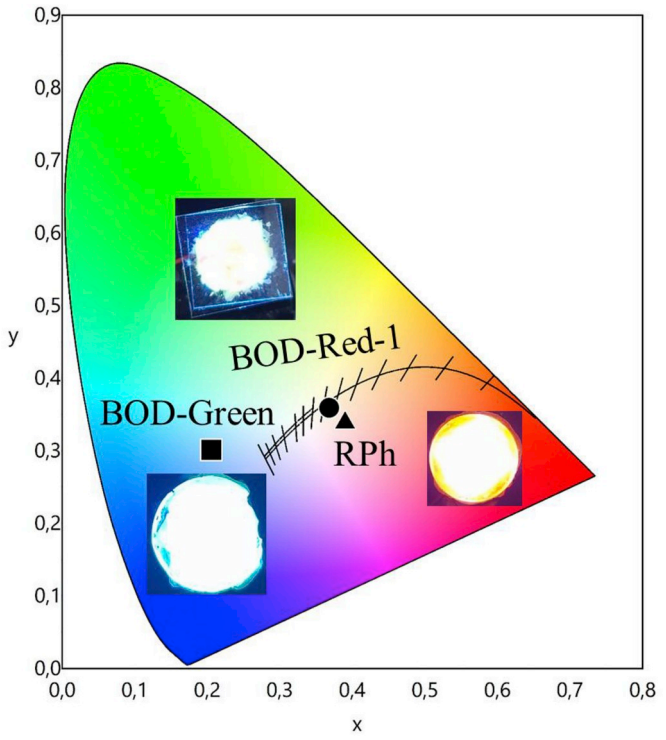

Fig. 7. CIE color coordinate diagram of the selected samples (one that showing the highest CRI) from the produced PDMS/PMMA-(BOD-Green) composite (square), RPh (triangle), and PDMS/PMMA-(BOD-Red-1) (circle). Photographs demonstrate the white light generation of the corresponding samples. (For interpretation of the references to color in this figure legend, the reader is referred to the Web version of this article.)

BOD-Red-1 fibers was prepared to test the stability of BOD-based color conversion layer against time under continous blue LED illumination. PL spectrum of the generated white light by this color conversion layer was collected at particular times from 0 to 390 min (Fig. S4), and peak intensities at 445, 530, and 610 nm were recorded in order to track the change of corresponding blue LED, BOD-Green, and BOD-Red-1 emission intensities in time, respectively. As a result, blue LED, BOD-Green, and BOD-Red-1 peak intensities were observed to be fitted to a linear curve that follows almost a straight line along the x-axis. In this sense, it can be claimed that the color conversion layer consisting of these BOD-based dyes are optically very stable against time under continous blue light illumination.

Commission Internationale de l'éclairage (CIE) color coordinates (presented explicitly in Table S2) of the selected two samples providing the highest CRI (sample 5 of both BOD-Red-1 and RPh), and one sample from the neat BOD-Green having 40 mg fiber mass (Fig. 3) were presented in Fig. 7. BOD-Green generates a cool white light, pointed with filled square, where the corresponding colour coordinates located at the region close to blue (inset figure, which is the photographic image of the generated white light over blue LED chip verifies this cool white light generation). On the other hand, samples containing PMMA-(BOD-Red-1) fibers and red phosphors (RPh) are located at the white light region shifted slightly towards yellow and red, respectively. They provide high CRI and low CCT. Corresponding photographic images of the both BOD-Red-1 and RPh verify the production of an explicit white light over blue LED chip.

4. Conclusion

BODIPY-based molecules having red and green colours were readily incorporated into fibrous PMMA via electrospinning and the fibers were embedded into PDMS matrix. The resulting composite shows promising conversion layer in WLED as an alternative to the current commercially used YAG:Ce^{3+} pigment particles. White light properties were found to be one of the best in literature and were found to be better than the commercial one. The problematic issue regarding with the usage of such organic molecules in WLED could be the aggregation of the individual molecules. Since the molecules undergo strong intermolecular π-π stacking, they may assemble into larger molecular structures due to that can reduce the optical features of the devices. Electrospinning was found to be the efficient method to achieve molecular dispersion such that molecules are confined into submicron diameter fibers. Since the aggregation of the dye molecules are reduced, better optical performance can be achieved particularly for white light generation.

Author contributions

The manuscript was written through contributions of all authors. All authors have given approval to the final version of the manuscript.

Appendix A. Supplementary data

Supplementary data to this article can be found online at https://doi.org/10.1016/j.dyepig.2019.107932.

References

[1] Cho J, et al. White light-emitting diodes: history, progress, and future. Laser Photonics Rev 2017.
[2] Katona TM, Pattison PM, Paolini S. Status of solid state lighting product development and future trends for general illumination. Annu Rev Chem Biomol Eng 2016;7:263–81.
[3] Schubert EF, et al. Solid-state lighting—a benevolent technology. Rep Prog Phys 2006;69(12):3069.
[4] Haitz R, Tsao JY. Solid-state lighting. Optik & Photonik 2011;6(2):26–30.
[5] Tsao JY, et al. Solid-state lighting: an energy-economics perspective. J Phys D Appl Phys 2010;43(35). 354001.
[6] Waide P, Tanishima S. Light's labour's lost: policies for energy-efficient lighting. OECD Publishing; 2006.
[7] Tan S, et al. Advances in the LED materials and architectures for energy-saving solid-state lighting toward "lighting revolution". IEEE Photonics J 2012;4(2):613–9.
[8] George NC, Denault KA, Seshadri R. Phosphors for solid-state white lighting. Annu Rev Mater Res 2013;43:481–501.
[9] Shur MS, Zukauskas R. Solid-state lighting: toward superior illumination. Proc IEEE 2005;93(10):1691–703.
[10] Steigerwald DA, et al. Illumination with solid state lighting technology. IEEE J Sel Top Quantum Electron 2002;8(2):310–20.
[11] Muthu S, Schuurmans FJ, Pashley MD. Red, green, and blue LEDs for white light illumination. IEEE J Sel Top Quantum Electron 2002;8(2):333–8.
[12] Xia Z, et al. Recent developments in the new inorganic solid-state LED phosphors. Dalton Trans 2016;45(28):11214–32.
[13] Ye S, et al. Phosphors in phosphor-converted white light-emitting diodes: recent advances in materials, techniques and properties. Mater Sci Eng R Rep 2010;71(1):1–34.
[14] Shinde K, Dhoble S. Europium-activated orthophosphate phosphors for energy-efficient solid-state lighting: a review. Crit Rev Solid State Mater Sci 2014;39(6):459–79.
[15] Lin CC, Liu R-S. Advances in phosphors for light-emitting diodes. J Phys Chem Lett 2011;2(11):1268–77.
[16] Güner T, Köseoğlu D, Demir MM. Multilayer design of hybrid phosphor film for application in LEDs. Opt Mater 2016;60:422–30.
[17] Narendran N, et al. Extracting phosphor-scattered photons to improve white LED efficiency. Phys Status Solidi 2005;202(6):R60–2.
[18] Allen SC, Steckl AJ. A nearly ideal phosphor-converted white light-emitting diode. Appl Phys Lett 2008;92(14). 143309.
[19] Lin CC, Meijerink A, Liu R-S. Critical red components for next-generation white LEDs. J Phys Chem Lett 2016;7(3):495–503.
[20] Li J, et al. Advanced red phosphors for white light-emitting diodes. J Mater Chem C 2016;4(37):8611–23.
[21] Jang E, et al. White-light-emitting diodes with quantum dot color converters for display backlights. Adv Mater 2010;22(28):3076–80.
[22] Di X, et al. Stable and brightly luminescent all-inorganic cesium lead halide perovskite quantum dots coated with mesoporous silica for warm WLED. Dyes Pigments 2017;146:361–7.
[23] Li G, et al. Solvent-polarity-engineered controllable synthesis of highly fluorescent cesium lead halide perovskite quantum dots and their use in white light-emitting diodes. Adv Funct Mater 2016;26(46):8478–86.
[24] Guner T, Demir MM. A review on halide perovskites as color conversion layers in white light emitting diode applications. Phys Status Solidi 2018;215(13):1800120.

[25] Meyns M, et al. Polymer-enhanced stability of inorganic perovskite nanocrystals and their application in color conversion LEDs. ACS Appl Mater Interfaces 2016;8(30):19579–86.
[26] Zhou J, et al. Inorganic halide perovskite quantum dot modified YAG-based white LEDs with superior performance. J Mater Chem C 2016;4(32):7601–6.
[27] He X, Qiu Y, Yang S. Fully-inorganic trihalide perovskite nanocrystals: a new research frontier of optoelectronic materials. Adv Mater 2017;29(32):1700775.
[28] Adjokatse S, Fang H-H, Loi MA. Broadly tunable metal halide perovskites for solid-state light-emission applications. Mater Today 2017.
[29] Guner T, et al. Perylene-embedded electrospun PS fibers for white light generation. Dyes Pigments 2019;160:501–8.
[30] Caruso F, et al. Generation of white LED light by frequency downconversion using perylene-based dye. Electron Lett 2012;48(22):1417–9.
[31] Kozma E, Mróz W, Galeotti F. A polystyrene bearing perylene diimide pendants with enhanced solid state emission for white hybrid light-emitting diodes. Dyes Pigments 2015;114:138–43.
[32] Galeotti F, et al. Tailorable perylene-loaded fluorescent nanostructures: a multifaceted approach enabling their application in white hybrid LEDs. J Mater Chem C 2016;4(23):5407–15.
[33] Findlay NJ, et al. An organic down-converting material for white-light emission from hybrid LEDs. Adv Mater 2014;26(43):7290–4.
[34] Taylor-Shaw E, et al. Cool to warm white light emission from hybrid inorganic/organic light-emitting diodes. J Mater Chem C 2016;4(48):11499–507.
[35] Pan G-H, et al. Dyes embedded YAG: Ce3+@ SiO2 composite phosphors toward warm wLEDs through radiative energy transfer: preparation, characterization and luminescence properties. Nanoscale 2018;10(47):22237–51.
[36] Luo D, et al. Regulating charge and exciton distribution in high-performance hybrid white organic light-emitting diodes with n-type interlayer switch. Nano-Micro Lett 2017;9(4):37.
[37] Liu B-Q, et al. Extremely high-efficiency and ultrasimplified hybrid white organic light-emitting diodes exploiting double multifunctional blue emitting layers. Light Sci Appl 2016;5(8):e16137.
[38] Liu B, et al. Manipulation of charge and exciton distribution based on blue aggregation-induced emission fluorophors: a novel concept to achieve high-performance hybrid white organic light-emitting diodes. Adv Funct Mater 2016;26(5):776–83.
[39] Luo D, et al. Extremely simplified, high-performance, and doping-free white organic light-emitting diodes based on a single thermally activated delayed fluorescent emitter. ACS Energy Lett 2018;3(7):1531–8.
[40] Caruso F, et al. Frequency-Downconversion stability of PMMA coatings in hybrid white light-emitting diodes. J Electron Mater 2016;45(1):682–7.
[41] Kajiwara Y, et al. Efficient simultaneous emission from RGB-emitting organoboron dyes incorporated into organic–inorganic hybrids and preparation of white light-emitting materials. J Mater Chem C 2013;1(29):4437–44.
[42] Fu B, et al. Label-free detection of pH based on the i-motif using an aggregation-caused quenching strategy. Chem Commun 2015;51(95):16960–3.
[43] Zhang Y, et al. Aggregation-induced emission luminogens as color converters for visible-light communication. ACS Appl Mater Interfaces 2018;10(40):34418–26.
[44] Birks JB. Photophysics of aromatic molecules. 1970.
[45] Ma X, et al. Fluorescence aggregation-caused quenching versus aggregation-induced emission: a visual teaching technology for undergraduate chemistry students. J Chem Educ 2015;93(2):345–50.
[46] Soper SA, Mattingly QL. Steady-state and picosecond laser fluorescence studies of nonradiative pathways in tricarbocyanine dyes: implications to the design of near-IR fluorochromes with high fluorescence efficiencies. J Am Chem Soc 1994;116(9):3744–52.
[47] Eggeling C, Volkmer A, Seidel CA. Molecular photobleaching kinetics of rhodamine 6G by one-and two-photon induced confocal fluorescence microscopy. ChemPhysChem 2005;6(5):791–804.
[48] Demir MM, et al. Electrospinning of polyurethane fibers. Polymer 2002;43(11):3303–9.
[49] Hong Y, Lam JW, Tang BZ. Aggregation-induced emission. Chem Soc Rev 2011;40(11):5361–88.
[50] Börgardts M, Müller TJ. Energy down converting organic fluorophore functionalized mesoporous silica hybrids for monolith-coated light emitting diodes. Beilstein J Org Chem 2017;13:768.
[51] Das S, Manam J. Fluorescein isothiocyanate and rhodamine B dye encapsulated mesoporous SiO 2 for applications of blue LED excited white LED. Opt Mater 2018;79:259–63.
[52] Qi X, et al. New BODIPY derivatives as OFF− ON fluorescent chemosensor and fluorescent chemodosimeter for Cu2+: cooperative selectivity enhancement toward Cu2+. J Org Chem 2006;71(7):2881–4.
[53] Sun W, Chen R, Marin L. Bodipy based chemosensors for highly sensitive and selective detection of Hg2+ ion. New J Chem 2018;42(23):19224–31.
[54] Wang L, Fang G, Cao D. A novel phenol-based BODIPY chemosensor for selective detection Fe3+ with colorimetric and fluorometric dual-mode. Sens Actuators B Chem 2015;207:849–57.
[55] Palao E, et al. Exploring the application of the Negishi reaction of haloBODIPYs: generality, regioselectivity, and synthetic utility in the development of BODIPY laser dyes. J Org Chem 2016;81(9):3700–10.
[56] Duran-Sampedro G, et al. First highly efficient and photostable E and C derivatives of 4, 4-Difluoro-4-bora-3a, 4a-diaza-s-indacene (BODIPY) as dye lasers in the liquid phase, thin films, and solid-state rods. Chem. Eur J. 2014;20(9):2646–53.
[57] Üçüncü M, et al. BODIPY–Au (I): a photosensitizer for singlet oxygen generation and photodynamic therapy. Org Lett 2017;19(10):2522–5.
[58] Erbas-Cakmak S, Akkaya EU. Toward singlet oxygen delivery at a measured rate: a self-reporting photosensitizer. Org Lett 2014;16(11):2946–9.
[59] Sayar M, et al. A BODIPY-based fluorescent probe to visually detect phosgene: toward the development of a handheld phosgene detector. Chem. Eur J. 2018;24(13):3136–40.
[60] Bottari G, et al. Covalent and noncovalent phthalocyanine− carbon nanostructure systems: synthesis, photoinduced electron transfer, and application to molecular photovoltaics. Chem Rev 2010;110(11):6768–816.
[61] Fan J, et al. Energy transfer cassettes based on organic fluorophores: construction and applications in ratiometric sensing. Chem Soc Rev 2013;42(1):29–43.
[62] Bozdemir OA, et al. Synthesis of symmetrical multichromophoric BODIPY dyes and their facile transformation into energy transfer cassettes. Chem. Eur J. 2010;16(21):6346–51.
[63] Zhang X, Xiao Y, Qian X. Highly efficient energy transfer in the light harvesting system composed of three kinds of boron− dipyrromethene derivatives. Org Lett 2008;10(1):29–32.
[64] Harriman A. Artificial light-harvesting arrays for solar energy conversion. Chem Commun 2015;51(59):11745–56.
[65] Ziessel R, et al. An artificial light-harvesting array constructed from multiple Bodipy dyes. J Am Chem Soc 2013;135(30):11330–44.
[66] Bonardi L, et al. Fine-tuning of yellow or red photo-and electroluminescence of functional difluoro-boradiazaindacene films. Adv Funct Mater 2008;18(3):401–13.
[67] Liu C-L, et al. Bodipy dyes bearing oligo (ethylene glycol) groups on the meso-phenyl ring: tuneable solid-state photoluminescence and highly efficient OLEDs. J Mater Chem C 2014;2(28):5471–8.
[68] Güner T, Şentürk U, Demir MM. Optical enhancement of phosphor-converted wLEDs using glass beads. Opt Mater 2017;72:769–74.
[69] Yuce H, et al. Phosphor-based white LED by various glassy particles: control over luminous efficiency. Opt Lett 2019;44(3):479–82.